Origin of Magnetic Ordering in a Structurally Perfect Quantum Kagome Antiferromagnet

T. Arh,[1,2] M. Gomilšek,[1,3] P. Prelovšek,[1] M. Pregelj,[1] M. Klanjšek,[1] A. Ozarowski,[4] S. J. Clark,[3] T. Lancaster,[3] W. Sun,[5] J.-X. Mi,[5] and A. Zorko[1,2,*]

[1]*Jožef Stefan Institute, Jamova c. 39, SI-1000 Ljubljana, Slovenia*
[2]*Faculty of Mathematics and Physics, University of Ljubljana, Jadranska u. 19, SI-1000 Ljubljana, Slovenia*
[3]*Centre for Materials Physics, Durham University, South Road, Durham DH1 3LE, United Kingdom*
[4]*National High Magnetic Field Laboratory, Florida State University, Tallahassee, Florida 32310, USA*
[5]*Fujian Provincial Key Laboratory of Advanced Materials, Department of Materials Science and Engineering, College of Materials, Xiamen University, Xiamen 361005, Fujian Province, People's Republic of China*

(Received 10 December 2019; accepted 12 June 2020; published 8 July 2020)

The ground state of the simple Heisenberg nearest-neighbor quantum kagome antiferromagnetic model is a magnetically disordered spin liquid, yet various perturbations may lead to fundamentally different states. Here we disclose the origin of magnetic ordering in the structurally perfect kagome material $YCu_3(OH)_6Cl_3$, which is free of the widespread impurity problem. *Ab initio* calculations and modeling of its magnetic susceptibility reveal that, similar to the archetypal case of herbertsmithite, the nearest-neighbor exchange is by far the dominant isotropic interaction. Dzyaloshinskii-Moriya (DM) anisotropy deduced from electron spin resonance, susceptibility, and specific-heat data is, however, significantly larger than in herbertsmithite. By enhancing spin correlations within kagome planes, this anisotropy is essential for magnetic ordering. Our study isolates the effect of DM anisotropy from other perturbations and unambiguously confirms the predicted phase diagram.

DOI: 10.1103/PhysRevLett.125.027203

Quantum spin liquids are magnetically disordered, yet highly entangled states, promoted by quantum fluctuations on some geometrically frustrated spin lattices [1]. A paradigm predicting such a state even at zero temperature is the two-dimensional (2D) nearest-neighbor quantum kagome antiferromagnetic model (KAFM) [2–4] represented by Heisenberg, i.e., isotropic J_1 exchange bonds between spin-1/2 sites in Fig. 1. Yet, even small perturbations to this simple model can stabilize fundamentally different ground states, as their influence is strongly amplified by frustration. Various factors, including further-neighbor exchange interactions [5–11], magnetic anisotropy [9–14], defects [14–16], and structural distortions [17] have been the focus of theoretical investigations in recent years. One of the seminal predictions that still calls for a clear experimental validation is a quantum critical point induced by Dzyaloshinskii-Moriya (DM) magnetic anisotropy, separating a spin liquid from a magnetically ordered ground state of KAFM [12]. Here we elucidate the role of the DM interaction in promoting correlations that lead to magnetic ordering in a material that closely realizes the KAFM.

Actual KAFM realizations are as a rule plagued by several perturbations, making the assessment of the individual roles of these perturbations challenging. A direct consequence of many effects being intertwined is that even the existence of a spin gap in the spin-liquid ground state of the KAFM remains unsettled. In fact, for the hitherto most intensively studied KAFM material herbertsmithite [24], indications of a finite gap [25] have been recently superseded by the conclusion that the gap is absent [26]. However, the effects of particular perturbations present in this material on its low-energy magnetism remain unknown. Relevant imperfections include sizable intersite ion mixing [27–29], large DM anisotropy [30], and subtle structural distortion away from perfect kagome symmetry [31,32]. On the contrary, in the recently synthesized KAFM material $YCu_3(OH)_6Cl_3$ [33] no structure-related perturbations are present; there is no Cu-Y intersite disorder [33] and the initially reported small Y-site disorder [33] is absent in high-resolution neutron diffraction of high-quality powder samples [34]. Therefore, the recent discoveries of static internal magnetic fields below $T_N = 12$ K [34,35] and magnetic Bragg peaks at low temperatures [36] are rather surprising. Initially, a broad maximum in specific heat at a notably higher temperature of $T_{\max} = 16$ K was also assigned to 3D ordering [35], causing a discrepancy with T_N where static internal fields appear. Experiments have further established that the average ordered Cu^{2+} magnetic moment of an otherwise regular 120° magnetic structure is strongly reduced [36] and is accompanied by persisting spin fluctuations even at the lowest temperatures [35]. The origin of such exotic magnetism is unknown, but even more fundamentally, the basic question of the magnetic-ordering mechanism present in this material remains unexplained. Since $YCu_3(OH)_6Cl_3$ is a unique KAFM material with a

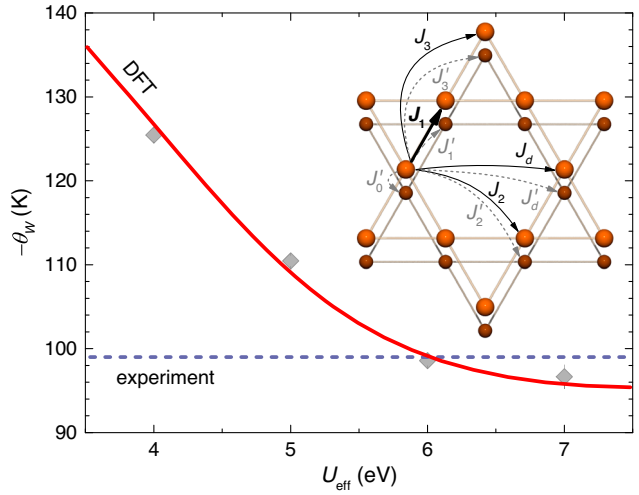

FIG. 1. Weiss temperature θ_W of $YCu_3(OH)_6Cl_3$ determined from DFT + U calculations for different values of the effective on-site Hubbard repulsion $U_{\rm eff}$ (points). The dashed line shows the experimental value $\theta_W = -99$ K, while the solid line serves as a guide to the eye. The inset depicts two neighboring kagome layers of Cu^{2+} spin-1/2 ions with in-plane Heisenberg exchange interactions J_i (solid arrows) and interplane interactions J_i' (dashed arrows). The nearest-neighbor coupling J_1 is by far the dominant one [18].

very limited number of possible perturbations, determining the ordering mechanism would be very important for assessing the impact of these perturbations on the spin-liquid ground state of KAFM.

Here we show a combination of density functional theory (DFT), finite-temperature Lanczos method (FTLM), and electron spin resonance (ESR) results, which allows us to address the origin of the unexpected magnetic ordering in $YCu_3(OH)_6Cl_3$. DFT calculations together with modeling of the magnetic susceptibility show that the nearest-neighbor Heisenberg exchange $J_1 = 82(2)$ K is by far the dominant isotropic interaction. Almost perfect agreement between numerical modeling and complementary ESR measurements, magnetic susceptibility, and specific heat data reveals an additional sizable out-of-plane DM anisotropy $D_z/J_1 = 0.25(1)$ that places the investigated compound in the magnetically ordered region of the KAFM phase diagram [12]. Moreover, FTLM modeling provides a novel insightful view into the role of DM interaction in KAFM and allows the precise determination of D_z, which is responsible for the maximum in specific heat at $T_{\rm max} = 16$ K related to the enhancement of 2D chiral spin correlations. 3D order is established via a small interlayer exchange below $T_N = 12$ K, where static internal magnetic fields appear [35].

To understand the magnetism of $YCu_3(OH)_6Cl_3$, the first task is to determine its dominant isotropic exchange interactions. As in other kagome compounds [37–40], we tackle this problem using total-energy (broken-symmetry) DFT + U calculations [41] (for details see Ref. [18]). We assume that each site is coupled with sites up to the third nearest neighbor in the kagome layer and with equivalent sites in the neighboring two kagome layers (Fig. 1). Our calculated exchange constants and the corresponding Weiss temperature $\theta_W = -\sum_i z_i J_i/4$, where z_i is the number of neighbors coupled to a particular site with J_i [42], depend on the effective on-site Hubbard repulsion $U_{\rm eff}$ [18]. θ_W is compared with its experimental value of $-99(1)$ K, which is obtained from a Curie-Weiss fit to the susceptibility data (inset in Fig. 2). The experiment is well reproduced for $U_{\rm eff} = 6$ eV (Fig. 1), a value consistent with previous studies on similar materials [37–40]. We find that the exchange interaction between nearest neighbors $J_1 = 84.2(4)$ K by far exceeds all other Heisenberg interactions, as all of them are below 5% of J_1, irrespective of the chosen value of $U_{\rm eff}$ [18].

Next, we focus on the temperature dependence of the magnetic susceptibility to verify that the calculated exchange constants are consistent with experiment. We first compare the experimental susceptibility [35] to a high temperature series expansion (HTSE) calculation for a simplified J_1–J_2–J_d model [43] in Fig. 2. The HTSE curve fitted in the temperature range between 100 and 300 K matches the experiment very well and yields the exchange constants $J_1 = 79.5(1)$, $J_2 = 2.8(27)$, and $J_d = 4.3(54)$ K. Furthermore, we can compare the experiment to FTLM calculations for a pure nearest-neighbor KAFM on a $N = 42$ spin cluster [44]. Good agreement is

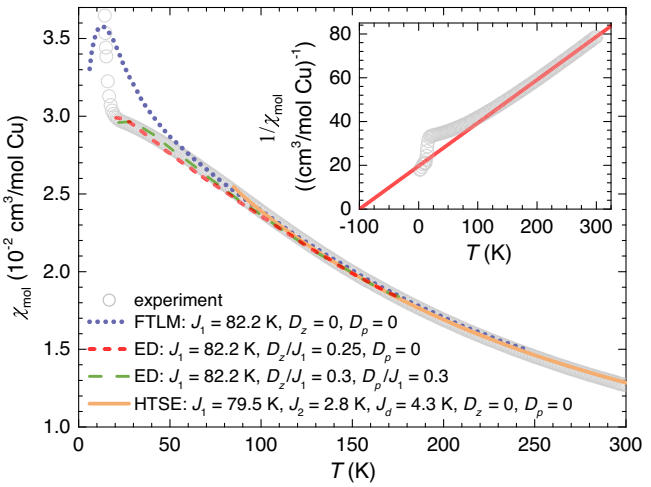

FIG. 2. Molar susceptibility $\chi_{\rm mol}$ of $YCu_3(OH)_6Cl_3$ in a field of 0.1 T [35], with its sharp increase at low temperatures indicating magnetic ordering. The solid line is a fit with the HTSE J_1–J_2–J_d model [43]. The dotted line shows FTLM calculations for isotropic KAFM on $N = 42$ sites [44]. The dashed lines are ED calculations with additional out-of-plane DM component D_z and in-plane component D_p for $N = 15$ sites [45], which are accurate to within 4% down to T_N [18]. The inset shows a Curie-Weiss analysis, $1/\chi_{\rm mol} = (T - \theta_W)/C$, with the Weiss temperature $\theta_W = -99$ K and g factor $g = 2.077$.

obtained for temperatures down to $0.6J_1 \sim 50$ K with $J_1 = 82.2(1)$ K being the only free parameter (Fig. 2).

The fact that all three independent approaches yield very similar predictions, namely, a dominant Heisenberg exchange interaction $J_1 = 82(2)$ K, gives strong credibility to these results. As isotropic exchange interactions beyond the nearest neighbors are limited to at most 5% of J_1, $YCu_3(OH)_6Cl_3$ can be placed alongside herbertsmithite [38] as one of the best realizations of the nearest-neighbor KAFM. In all other well-studied examples, like kapellasite [37,39,43], haydeeite [37,39,46], volborthite [47], and vesignieite [48], further-neighbor interactions are much larger. As interactions $|J_2|, |J_3|, |J_d| \gtrsim 0.2J_1$ [5–7,9] or $|J'| \gtrsim 0.15J_1$ [8] are needed to induce magnetic ordering in the KAFM, these are evidently too small in $YCu_3(OH)_6Cl_3$. The only remaining perturbation that can account for its ordered ground state is magnetic anisotropy. Since there are no symmetry restrictions [49], both the antisymmetric DM and the symmetric anisotropic exchange (AE) interaction are allowed. However, DM anisotropy is generally dominant in Cu^{2+}-based magnets because it is a one order lower correction to the isotropic exchange [49], so that the AE term is smaller by a factor $\Delta g/g \sim 0.2$ [50]. Here Δg is the shift of the g factor from the free electron value. Furthermore, as the easy-plane AE interaction that would be compatible with the observed planar magnetic order [36] does not lead to ordering of the KAFM [13,51], we expect the DM interaction to play a dominant role.

The next task is, therefore, to determine the DM interaction $\mathbf{D} \cdot (\mathbf{S}_i \times \mathbf{S}_j)$ between the nearest neighbors. First, we note that further-neighbor isotropic exchange interactions are too small to account for the large discrepancy between the experimental magnetic susceptibility and the nearest-neighbor FTLM calculations already at temperatures as high as $0.6J_1 \sim 50$ K (Fig. 2). On the contrary, a sizable DM interaction can explain this deviation. Indeed, according to exact-diagonalization (ED) calculations [45], the out-of-plane component D_z suppresses susceptibility compared to the isotropic KAFM, while the in-plane component D_p enhances it [18]. The experimental suppression is well reproduced for $D_z/J_1 = 0.25(1)$ all the way down to the ordering temperature if $D_p = 0$ (Fig. 2). For $D_p > 0$ a larger D_z is required [18], e.g., for $D_p/J_1 = 0.30$ one finds $D_z/J_1 = 0.30(1)$ (Fig. 2).

We can place further constraints on the magnitude of both DM components based on ESR results (for details see Ref. [18]), as magnetic anisotropy directly broadens the ESR spectra [52]. The measured spectra [18] are broader than in other Cu-based kagome compounds like herbertsmithite [30], vesignieite [53], and kapellasite [54] by almost an order of magnitude. Above 200 K the ESR linewidth is constant at $\Delta B = 6.8(5)$ T (inset in Fig. 3), which is consistent with the high-temperature paramagnetic regime and allows for the application of Kubo-Tomita (KT) theory [55]. The well-established expression for the ESR linewidth on the kagome lattice [30,53] allows us to derive the $D_z(D_p)$ solution [18] shown in Fig. 3. Contrary to the case of susceptibility, which is affected oppositely by the two DM components, they both broaden the ESR linewidth. The total magnitude of the DM vector is therefore approximately limited by $D/J_1 \simeq [2g\mu_B\Delta B/(\sqrt{\pi}k_BJ_1)]^{1/2} = 0.36$, where k_B is the Boltzmann constant and μ_B is the Bohr magneton. The joint ESR and susceptibility analysis yields the limits $0.25 < D_z/J_1 < 0.29$ and $D_p/J_1 < 0.15$ (Fig. 3). We note, though, that in accordance with recent ED calculations demonstrating that the KT approach might somewhat overestimate the DM anisotropy on the kagome lattice [56], the true DM components should be closer to the lower limits, $D_z/J_1 = 0.25$ and $D_p/J_1 \simeq 0$.

An independent check of the above estimates is provided by modeling previously published zero-field specific heat (c) data [35]. FTLM calculations [57,58] of the magnetic contribution to the specific heat c_m, which were performed on spin clusters with up to $N = 30$ spins for various D_z/J_1 and D_p/J_1 ratios (for details see Ref. [18]), reveal two well-resolved maxima in c_m for $D_z/J_1 \gtrsim 0.08$ [Fig. 4(a)], as previously also observed in ED calculations on smaller clusters [45]. A broad high-temperature maximum is, similarly to the spin-1/2 square lattice [59], found around $0.67J_1$ and does not shift with the DM interaction. Therefore, it is associated with the enhancement of nearest-neighbor spin correlations [60,61]. On the contrary, a much narrower low-temperature maximum shifts almost linearly with the out-of-plane DM component and is found

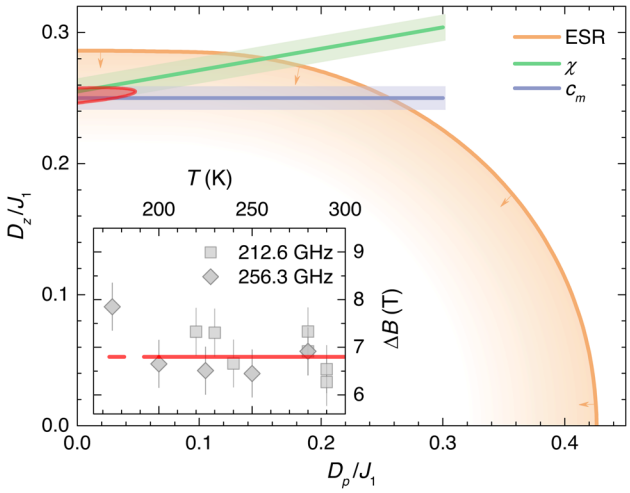

FIG. 3. The interdependence of both DM components in $YCu_3(OH)_6Cl_3$ based on the analysis of the ESR linewidth (shown in the inset), magnetic susceptibility, and specific heat. Shaded regions show experimental uncertainty, while the arrows imply that ESR only gives an upper bound. The red area is the region with globally acceptable parameters, where the solid red line indicates the 1-sigma boundary.

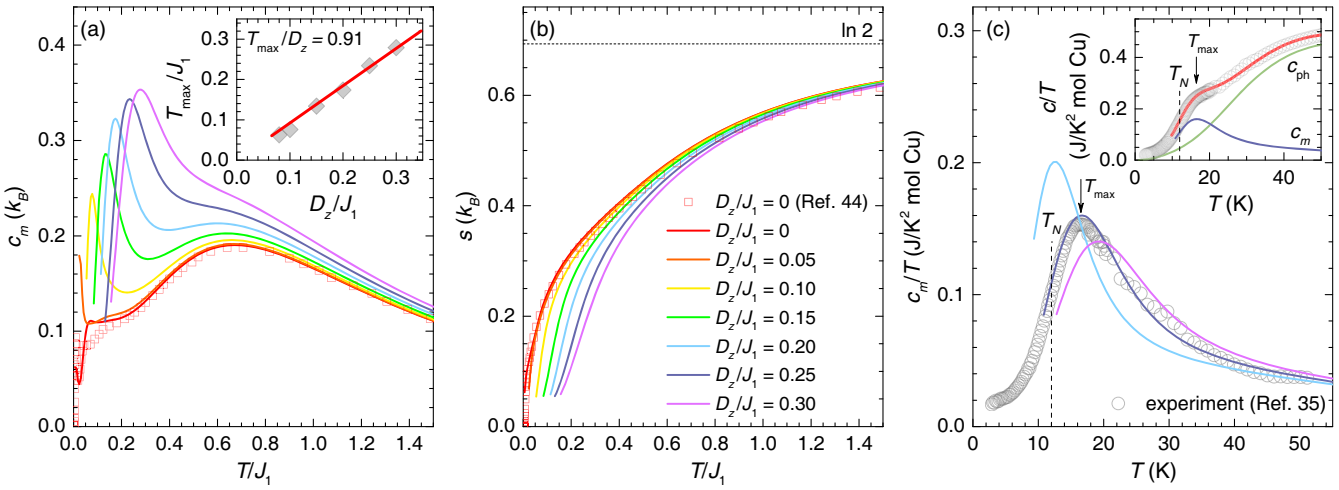

FIG. 4. The temperature dependence of (a) the magnetic specific heat c_m and (b) the entropy per site s in zero magnetic field obtained from the FTLM calculations on $N = 30$ spin clusters for various D_z values (lines). The data are shown only for temperatures where $s \geq 0.07 k_B$ [18]. The results from Ref. [44] obtained on $N = 42$ spin clusters for $D_z/J_1 = 0$ are shown for comparison (symbols). The inset in (a) shows the variation of the low-temperature c_m maximum position $T_{\max}$ with D_z/J_1. (c) Selected FTLM calculations of c_m/T compared to the experimental data (circles). The inset shows the total specific heat of $YCu_3(OH)_6Cl_3$ (circles; data taken from Ref. [35]) and the fit (red line) composed of the magnetic contribution for $D_z/J_1 = 0.25$ (blue line) and a phonon contribution (green line) [18]. The arrow indicates $T_{\max} = 16$ and the dashed line $T_N = 12$ K.

at $T_{\max} \simeq 0.91 D_z$ [inset in Fig. 4(a)]. In sharp contrast, c_m is almost insensitive to the in-plane DM component at least up to $D_p/J_1 \leq 0.3$ [18,45]. As the D_z term linearly shifts the energy of the 120° spin structure of basic kagome triangles [36] while D_p does not, we attribute the low-temperature maximum to growing chiral spin correlations within the kagome planes. This makes specific heat a unique probe of the DM component D_z on the kagome lattice, which is much more sensitive [Fig. 4(c)] than magnetic susceptibility [18].

For $D_z/J_1 = 0.25$, the predicted magnetic specific heat nicely matches the experiment [Fig. 4(c)]. Indeed, we can fit the c/T data very well with the model $c = c_m + c_{\rm ph}$ that includes a phonon contribution $c_{\rm ph}$. The fit is already good for a simple Debye phonon model with the Debye temperature $\theta_D = 224(5)$ K and is further improved by including an additional Einstein phonon contribution [inset in Fig. 4(c)] [18], corresponding to a Raman active mode at 123 cm^{-1}, as found in structurally similar herbertsmithite [62]. The obtained $D_z/J_1 = 0.25(1)$ is in excellent agreement with the lower-bound estimate based on ESR and susceptibility modeling (Fig. 3) and thus provides further evidence that the in-plane DM component is much smaller, i.e., $D_p/J_1 < 0.05$. Although the DM anisotropy in $YCu_3(OH)_6Cl_3$ is larger than in some other Cu^{2+}-based KAFM materials [30,53], its size is compatible with the order-of-magnitude estimate [49] $D_z/J_1 \sim \Delta g/g \sim 0.2$ for the Cu^{2+} ions [50].

Having established the main terms in the spin Hamiltonian of $YCu_3(OH)_6Cl_3$, we are now in position to discuss the origin of its magnetic ordering. It is theoretically well established that the out-of-plane DM interaction leads to a $q = 0$ long-range order of KAFM at zero temperature if its strength exceeds the critical value $D_z^c = 0.10(2) J_1$ [9,10,12,14] separating the spin liquid and the ordered phase. Contrary to the paradigmatic KAFM material herbertsmithite, which appears to be on the verge of criticality [30], we find that $YCu_3(OH)_6Cl_3$ lies well inside the ordered phase. Nevertheless, the average ordered moment should be strongly suppressed due to quantum fluctuations. Indeed, the predicted moment of 0.35 μ_B for $D_z/J_1 = 0.25$ [12] matches reasonably well with the experimental value of 0.42(2) μ_B [36].

Finally, let us comment on the compatibility of our results with the celebrated Mermin-Wagner theorem [63], which precludes long-range order in the considered 2D model at nonzero temperatures due to continuous in-plane symmetry. As revealed by FTLM calculations, 2D short-range chiral order is established below $T_{\max} = 16$ K, while 3D order is only established below $T_N = 12$ K [Fig. 4(c)], where static internal magnetic fields appear, the longitudinal muon spin relaxation rate suddenly starts increasing and bulk susceptibility exhibits a clear cusp (see Fig. 6 in Ref. [18]). Finite T_N requires additional interlayer interactions J' and is determined by the growth of the in-plane correlation length ξ to the extent that the thermal energy drops below the interaction energy of short-range ordered 2D regions on neighboring kagome planes, when $T_N \approx [\xi(T_N)/d]^2 J' S(S+1)$, with d being the nearest-neighbor distance [60,61]. As ξ should only marginally depend on the interlayer interaction for $J'/J_1 \ll 1$ and thus T_N should only logarithmically depend on J' [59,61,64],

T_N is dominantly determined by D_z in $YCu_3(OH)_6Cl_3$. This anisotropy promotes building up of 2D chiral spin correlations, which corresponds to effectively shifting a large release of the system's entropy to temperatures around $T_{\max} \approx D_z$ [Fig. 4(b)]. As a result, for $J'/J_1 \ll 1$ yielding $T_N < T_{\max}$ most of the entropy is already released around $T_{\max}$ and the effective number of degrees of freedom involved in 3D ordering is significantly reduced, making the cusp in c_m at T_N unobservable [59]. Thus, 2D physics essentially prevails down to T_N and justifies the absence of any cluster-size dependence of the c_m curves in FTLM calculations [18].

In conclusion, $YCu_3(OH)_6Cl_3$ turns out to be an extremely rare structurally perfect KAFM material, with the nearest-neighbor isotropic exchange interaction $J_1 = 82(2)$ K dominating all other isotropic interactions, while by far the most relevant perturbation is the out-of-plane DM anisotropy $D_z/J_1 = 0.25(1)$. This is determined from a perfect coincidence of the experiments and numerical calculations for the two most common bulk magnetic characterization techniques as well as ESR, which is unique in the field of frustrated magnetism. Such D_z/J places the system in the magnetically ordered part of the predicted phase diagram [12]. This provides an unambiguous experimental confirmation of the key role of the DM interaction in inducing magnetic order on the kagome lattice. Furthermore, now that this role is well understood, a sister compound $Y_3Cu_9(OH)_{18}OCl_8$ with a slightly distorted kagome lattice and apparently a spin-liquid ground state [34] provides an ideal opportunity to study the effects of further perturbations. Since in this compound very similar exchange interactions and magnetic anisotropy as in $YCu_3(OH)_6Cl_3$ are expected, the reasoning for its lack of magnetic ordering should be searched in deviations from perfect kagome symmetry.

The authors thank O. Cépas, F. Bert, and P. Mendels for fruitful discussions. This work was supported by the Slovenian Research Agency under Projects No. BI-US/18-20-064, No. Z1-1852, and Program No. P1-0125. M. G., T. L. and S. J. C. are grateful to EPSRC (UK) for financial support through Grant No. EP/N024028/1. The National High Magnetic Field Laboratory is supported by National Science Foundation through NSF/DMR-1644779 and the State of Florida. Computing resources were provided by the F1 department at IJS, STFC Scientific Computing Department's SCARF cluster and the Durham HPC Hamilton cluster. Research data from the UK effort will be made available via Durham Collections.

*andrej.zorko@ijs.si

[1] *Introduction to Frustrated Magnetism: Materials, Experiments, Theory*, edited by C. Lacroix, P. Mendels, and F. Mila (Springer Verlag, Berlin, 2011).

[2] L. Balents, Spin liquids in frustrated magnets, Nature (London) **464**, 199 (2010).

[3] L. Savary and L. Balents, Quantum spin liquids: A review, Rep. Prog. Phys. **80**, 016502 (2017).

[4] Y. Zhou, K. Kanoda, and T.-K. Ng, Quantum Spin Liquid States, Rev. Mod. Phys. **89**, 025003 (2017).

[5] R. Suttner, C. Platt, J. Reuther, and R. Thomale, Renormalization group analysis of competing quantum phases in the J_1-J_2 Heisenberg model on the kagome lattice, Phys. Rev. B **89**, 020408(R) (2014).

[6] S.-S. Gong, W. Zhu, L. Balents, and D. N. Sheng, Global phase diagram of competing ordered and quantum spin-liquid phases on the kagome lattice, Phys. Rev. B **91**, 075112 (2015).

[7] S. Bieri, C. Lhuillier, and L. Messio, Projective symmetry group classification of chiral spin liquids, Phys. Rev. B **93**, 094437 (2016).

[8] O. Götze and J. Richter, The route to magnetic order in the spin-1/2 kagome Heisenberg antiferromagnet: The role of interlayer coupling, Europhys. Lett. **114**, 67004 (2016).

[9] M. Hering and J. Reuther, Functional renormalization group analysis of Dzyaloshinsky-Moriya and Heisenberg spin interactions on the kagome lattice, Phys. Rev. B **95**, 054418 (2017).

[10] W. Zhu, S.-S. Gong, and D. N. Sheng, Identifying spinon excitations from dynamic structure factor of spin-1/2 Heisenberg antiferromagnet on the Kagome lattice, Proc. Natl. Acad. Sci. U.S.A. **116**, 5437 (2019).

[11] B. Bernu, L. Pierre, K. Essafi, and L. Messio, Effect of perturbations on the kagome $S = 1/2$ antiferromagnet at all temperatures, Phys. Rev. B **101**, 140403 (2020).

[12] O. Cépas, C. M. Fong, P. W. Leung, and C. Lhuillier, Quantum phase transition induced by Dzyaloshinskii-Moriya interactions in the kagome antiferromagnet, Phys. Rev. B **78**, 140405(R) (2008).

[13] A. L. Chernyshev and M. E. Zhitomirsky, Quantum Selection of Order in an XXZ Antiferromagnet on a Kagome Lattice, Phys. Rev. Lett. **113**, 237202 (2014).

[14] I. Rousochatzakis, S. R. Manmana, A. M. Läuchli, B. Normand, and F. Mila, Dzyaloshinskii-Moriya anisotropy and nonmagnetic impurities in the $s = 1/2$ kagome system $ZnCu_3(OH)_6Cl_2$, Phys. Rev. B **79**, 214415 (2009).

[15] R. R. P. Singh, Valence Bond Glass Phase in Dilute Kagome Antiferromagnets, Phys. Rev. Lett. **104**, 177203 (2010).

[16] H. Kawamura, K. Watanabe, and T. Shimokawa, Quantum spin-liquid behavior in the spin-$\frac{1}{2}$ random-bond Heisenberg antiferromagnet on the kagome lattice, J. Phys. Soc. Jpn. **83**, 103704 (2014).

[17] M. R. Norman, N. J. Laurita, and D. Hsieh, Valence bond phases of herbertsmithite and related copper kagome materials, Phys. Rev. Research **2**, 013055 (2020).

[18] See Supplemental Material at http://link.aps.org/supplemental/10.1103/PhysRevLett.125.027203 for details on DFT and FTLM calculations, ESR measurements and analysis, modeling of the magneetic susceptibility and specific heat, as well as differentiating between $T_{\max}$ and T_N. This material includes Refs. [19–23].

[19] S. J. Clark, M. D. Segall, C. J. Pickard, P. J. Hasnip, M. J. Probert, K. Refson, and M. C. Payne, First principles methods using CASTEP, Z. Kristall. **220**, 567 (2005).

[20] S. Sharma, E. K. U. Gross, A. Sanna, and J. K. Dewhurst, Source-free exchange-correlation magnetic fields in density functional theory, J. Chem. Theory Comput. **14**, 1247 (2018).

[21] J. P. Perdew, K. Burke, and M. Ernzerhof, Generalized Gradient Approximation Made Simple, Phys. Rev. Lett. **77**, 3865 (1996).

[22] P. Prelovšek and J. Bonča, Ground state and finite temperature Lanczos methods, in *Strongly Correlated Systems—Numerical Methods*, edited by A. Avella and F. Mancini (Springer, Berlin, 2013).

[23] A. Tari, *The Specific Heat of Matter at Low Temperatures* (Imperial College, London, 2003).

[24] M. R. Norman, Colloquium: Herbertsmithite and the search for the quantum spin liquid, Rev. Mod. Phys. **88**, 041002 (2016).

[25] M. Fu, T. Imai, T.-H. Han, and Y. S. Lee, Evidence for a gapped spin-liquid ground state in a kagome Heisenberg antiferromagnet, Science **350**, 655 (2015).

[26] P. Khuntia, M. Velazquez, Q. Barthélemy, F. Bert, E. Kermarrec, A. Legros, B. Bernu, L. Messio, A. Zorko, and P. Mendels, Gapless ground state in the archetypal quantum kagome antiferromagnet $ZnCu_3(OH)_6Cl_2$, Nat. Phys. **16**, 469 (2020).

[27] M. A. de Vries, K. V. Kamenev, W. A. Kockelmann, J. Sanchez-Benitez, and A. Harrison, Magnetic Ground State of an Experimental $S = 1/2$ Kagome Antiferromagnet, Phys. Rev. Lett. **100**, 157205 (2008).

[28] A. Olariu, P. Mendels, F. Bert, F. Duc, J. C. Trombe, M. A. de Vries, and A. Harrison, ^{17}O NMR Study of the Intrinsic Magnetic Susceptibility and Spin Dynamics of the Quantum Kagome Antiferromagnet $ZnCu_3(OH)_6Cl_2$, Phys. Rev. Lett. **100**, 087202 (2008).

[29] D. E. Freedman, T. H. Han, A. Prodi, P. Müller, Q.-Z. Huang, Y.-S. Chen, S. M. Webb, Y. S. Lee, T. M. McQueen, and D. G. Nocera, Site specific X-ray anomalous dispersion of the geometrically frustrated kagome magnet, herbertsmithite, $ZnCu_3(OH)_6Cl_2$, J. Am. Chem. Soc. **132**, 16185 (2010).

[30] A. Zorko, S. Nellutla, J. van Tol, L. C. Brunel, F. Bert, F. Duc, J.-C. Trombe, M. A. de Vries, A. Harrison, and P. Mendels, Dzyaloshinsky-Moriya Anisotropy in the Spin-1/2 Kagome Compound $ZnCu_3(OH)_6Cl_2$, Phys. Rev. Lett. **101**, 026405 (2008).

[31] A. Zorko, M. Herak, M. Gomilšek, J. van Tol, M. Velázquez, P. Khuntia, F. Bert, and P. Mendels, Symmetry Reduction in the Quantum Kagome Antiferromagnet Herbertsmithite, Phys. Rev. Lett. **118**, 017202 (2017).

[32] N. J. Laurita, A. Ron, J. W. Han, A. Scheie, J. P. Sheckelton, R. W. Smaha, W. He, J.-J. Wen, J. S. Lee, Y. S. Lee, M. R. Norman, and D. Hsieh, Evidence for a parity broken monoclinic ground state in the $S = 1/2$ Kagomé antiferromagnet herbertsmithite, arXiv:1910.13606.

[33] W. Sun, Y.-X. Huang, S. Nokhrin, Y. Pan, and J.-X. Mi, Perfect Kagomé lattices in $YCu_3(OH)_6Cl_3$: A new candidate for the quantum spin liquid state, J. Mater. Chem. C **4**, 8772 (2016).

[34] Q. Barthélemy, P. Puphal, K. M. Zoch, C. Krellner, H. Luetkens, C. Baines, D. Sheptyakov, E. Kermarrec, P. Mendels, and F. Bert, Local study of the insulating quantum kagome antiferromagnets $YCu_3(OH)_6O_xCl_{3-x}$ ($x = 0, 1/3$), Phys. Rev. Mater. **3**, 074401 (2019).

[35] A. Zorko, M. Pregelj, M. Klanjšek, M. Gomilšek, Z. Jagličić, J. S. Lord, J. A. T. Verezhak, T. Shang, W. Sun, and J-X. Mi, Coexistence of magnetic order and persistent spin dynamics in a quantum kagome antiferromagnet with no intersite mixing, Phys. Rev. B **99**, 214441 (2019).

[36] A. Zorko, M. Pregelj, M. Gomilšek, M. Klanjšek, O. Zaharko, W. Sun, and J-X. Mi, Negative-vector-chirality 120° spin structure in the defect- and distortion-free quantum kagome antiferromagbet $YCu_3(OH)_6Cl_3$, Phys. Rev. B **100**, 144420 (2019).

[37] O. Janson, J. Richter, and H. Rosner, Modified Kagome Physics in the Natural Spin-1/2 Kagome Lattice Systems: Kapellasite $Cu_3Zn(OH)_6Cl_2$ and Haydeeite $Cu_3Mg(OH)_6Cl_2$, Phys. Rev. Lett. **101**, 106403 (2008).

[38] H. O. Jeschke, F. Salvat-Pujol, and R. Valentí, First-principles determination of Heisenberg Hamiltonian parameters for the spin-1/2 kagome antiferromagnet $ZnCu_3(OH)_6Cl_2$, Phys. Rev. B **88**, 075106 (2013).

[39] Y. Iqbal, H. O. Jeschke, J. Reuther, R. Valentí, I. I. Mazin, M. Greiter, and R. Thomale, Paramagnetism in the kagome compounds $(Zn, Mg, Cd)Cu_3(OH)_6Cl_2$, Phys. Rev. B **92**, 220404(R) (2015).

[40] H. O. Jeschke, F. Salvat-Pujol, E. Gati, N. H. Hoang, B. Wolf, M. Lang, J. A. Schlueter, and R. Valentí, Barlowite as a canted antiferromagnet: Theory and experiment, Phys. Rev. B **92**, 094417 (2015).

[41] K. Riedl, Y. Li, R. Valentí, and S. M. Winter, Ab initio approaches for low-energy spin Hamiltonians, Phys. Status Solidi B **256**, 1800684 (2019).

[42] J. B. Goodenough, *Magnetism and Chemical Bond* (Interscience Publishers, New York, 1963), Vol. 1.

[43] B. Bernu, C. Lhuillier, E. Kermarrec, F. Bert, P. Mendels, R. H. Colman, and A. S. Wills, Exchange energies of kapellasite from high-temperature series analysis of the kagome lattice J_1-J_2-J_d-Heisenberg model, Phys. Rev. B **87**, 155107 (2013).

[44] J. Schnack, J. Schulenburg, and J. Richter, Magnetism of the $N = 42$ kagome lattice antiferromagnet, Phys. Rev. B **98**, 094423 (2018).

[45] M. Rigol and R. R. P. Singh, Kagome lattice antiferromagnets and Dzyaloshinsky-Moriya interactions, Phys. Rev. B **76**, 184403 (2007).

[46] D. Boldrin, B. Fåk, M. Enderle, S. Bieri, J. Ollivier, S. Rols, P. Manuel, and A. S. Wills, Haydeeite: A spin-1/2 kagome ferromagnet, Phys. Rev. B **91**, 220408(R) (2015).

[47] O. Janson, S. Furukawa, T. Momoi, P. Sindzingre, J. Richter, and K. Held, Magnetic Behavior of Volborthite $Cu_3V_2O_7(OH)_2 \cdot 2H_2O$ Determined by Coupled Trimers Rather than Frustrated Chains, Phys. Rev. Lett. **117**, 037206 (2016).

[48] D. Boldrin, B. Fåk, E. Canévet, J. Ollivier, H. C. Walker, P. Manuel, D. D. Khalyavin, and A. S. Wills, Vesignieite: An $S = 1/2$ Kagome Antiferromagnet with Dominant Third-Neighbor Exchange, Phys. Rev. Lett. **121**, 107203 (2018).

[49] T. Moriya, Anisotropic superexchange interaction and weak ferromagnetism, Phys. Rev. **120**, 91 (1960).

[50] A. Abragam and B. Bleaney, *Electron Paramagnetic Resonance of Transition Ions* (Clarendon Press, Oxford, 1970).

[51] Y.-C. He and Y. Chen, Distinct Spin Liquids and Their Transitions in Spin-1/2 *XXZ* Kagome Antiferromagnets, Phys. Rev. Lett. **114**, 037201 (2015).

[52] A. Zorko, Determination of magnetic anisotropy by EPR, in *Topics From EPR Research*, edited by A. M. Maghraby (IntechOpen, London, 2019).

[53] A. Zorko, F. Bert, A. Ozarowski, J. van Tol, D. Boldrin, A. S. Wills, and P. Mendels, Dzyaloshinsky-Moriya interaction in vesignieite: A route to freezing in a quantum kagome antiferromagnet, Phys. Rev. B **88**, 144419 (2013).

[54] E. Kermarrec, A. Zorko, F. Bert, R. H. Colman, B. Koteswararao, F. Bouquet, P. Bonville, A. Hillier, A. Amato, J. van Tol, A. Ozarowski, A. S. Wills, and P. Mendels, Spin dynamics and disorder effects in the $S = 1/2$ kagome Heisenberg spin-liquid phase of kapellasite, Phys. Rev. B **90**, 205103 (2014).

[55] R. Kubo and K. Tomita, A general theory of magnetic resonance absorption, J. Phys. Soc. Jpn. **9**, 888 (1954).

[56] S. El Shawish, O. Cépas, and S. Miyashita, Electron spin resonance in $S = 1/2$ antiferromagnets at high temperature, Phys. Rev. B **81**, 224421 (2010).

[57] J. Jaklič and P. Prelovšek, Finite-temperature conductivity in the planar $t - J$ model, Phys. Rev. B **50**, 7129 (1994).

[58] J. Jaklič and P. Prelovšek, Finite-temperature properties of doped antiferromagnets, Adv. Phys. **49**, 1 (2000).

[59] P. Sengupta, A. W. Sandvik, and R. R. P. Singh, Specific heat of quasi-two-dimensional antiferromagnetic Heisenberg models with varying interplanar couplings, Phys. Rev. B **68**, 094423 (2003).

[60] S. Chakravarty, B. I. Halperin, and D. R. Nelson, Low-Temperature Behavior of Two-Dimensional Quantum Antiferromagnets, Phys. Rev. Lett. **60**, 1057 (1988).

[61] S. Chakravarty, B. I. Halperin, and D. R. Nelson, Two-dimensional quantum Heisenberg antiferromagnet at low temperatures, Phys. Rev. B **39**, 2344 (1989).

[62] D. Wulferding, P. Lemmens, P. Scheib, J. Röder, P. Mendels, S. Chu, T. Han, and Y. S. Lee, Interplay of thermal and quantum spin fluctuations in the kagome lattice compound herbertsmithite, Phys. Rev. B **82**, 144412 (2010).

[63] N. D. Mermin and H. Wagner, Absence of Ferromagnetism or Antiferromagnetism in One-or Two-Dimensional Isotropic Heisenberg Models, Phys. Rev. Lett. **17**, 1133 (1966).

[64] C. Yasuda, S. Todo, K. Hukushima, F. Alet, M. Keller, M. Troyer, and H. Takayama, Néel Temperature of Quasi-Low-Dimensional Heisenberg Antiferromagnets, Phys. Rev. Lett. **94**, 217201 (2005).